LANGMUIR

pubs.acs.org/Langmuir Article

Surface Pressure—Area Mechanics of Water-Spread Poly(ethylene glycol)-Based Block Copolymer Micelle Monolayers at the Air—Water Interface: Effect of Hydrophobic Block Chemistry

Seyoung Kim, Sungwan Park, Daniel J. Fesenmeier, Taesuk Jun, Kaustabh Sarkar, and You-Yeon Won*



Cite This: Langmuir 2023, 39, 13546-13559



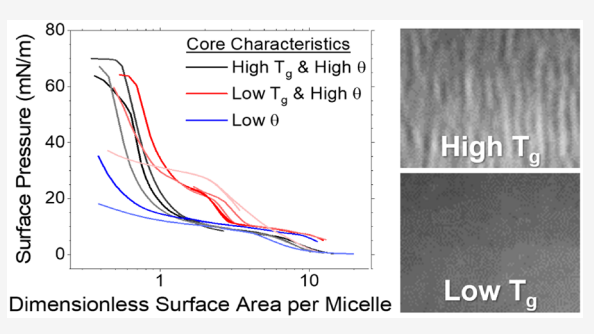
ACCESS I

III Metrics & More

Article Recommendations

Supporting Information

ABSTRACT: Amphiphilic block copolymer micelles can mimic the ability of natural lung surfactant to reduce the air—water interfacial tension close to zero and prevent the Laplace pressure-induced alveolar collapse. In this work, we investigated the air—water interfacial behaviors of polymer micelles derived from eight different poly(ethylene glycol) (PEG)-based block copolymers having different hydrophobic block chemistries to elucidate the effect of the core block chemistry on the surface mechanics of the block copolymer micelles. Aqueous micelles of about 30 nm in hydrodynamic diameter were prepared from the PEG-based block copolymers via equilibration—nanoprecipitation (ENP) and spread on the water surface using water as the spreading medium. Surface



pressure—area isotherm and quantitative Brewster angle microscopy (QBAM) measurements were performed to investigate how the micelle/monolayer structures change during lateral compression of the monolayer; widely varying structural behaviors were observed, including the wrinkling/collapse of micelle monolayers and deformation and/or the desorption of individual micelles. By bivariate correlation regression analysis of surface pressure—area isotherm data, it was found that the rigidity and hydrophobicity of the hydrophobic core domain, which are quantified by glass-transition temperature ($T_{\rm g}$) and water contact angle (θ) measurements, respectively, are coupled factors that need to be taken into account concurrently in order to control the surface mechanical properties of polymer micelle monolayers; micelles having rigid and strongly hydrophobic cores exhibited high surface pressure and a high compressibility modulus under high compression. High surface pressure and a high compressibility modulus were also found to be correlated with the formation of wrinkles in the micelle monolayer (visualized by Brewster angle microscopy (BAM)). From this study, we conclude that polymer micelles based on hydrophobic block materials having higher $T_{\rm g}$ and θ are more suitable for surfactant replacement therapy applications that require the therapeutic surfactant to produce a high surface pressure and modulus at the alveolar air—water interface.

INTRODUCTION

Nature uses mixtures of lipids having different hydrophobic tails (acyl chains of varying unsaturation and length) to construct molecular membranes that perform specific desired functions. For instance, most of the fatty acids that constitute the plasma membranes of cells are mono- or polyunsaturated fatty acids so that they can impart fluidity to the lipid membrane. On the other hand, a saturated lipid, dipalmitoylphosphatidylcholine (DPPC), is enriched to up to 40% of the total lipid content in the alveoli in order to be able to reduce the surface tension of the alveolar lipid monolayer down close to zero at end expiration.^{2,3} Similarly, Langmuir monolayers of synthetic homopolymers⁴⁻⁶ and block copolymers^{7,8} have been shown to exhibit a wide range of surface mechanical behavior depending on the relaxation dynamics of the polymer molecules. However, using synthetic polymers to control the surface mechanical properties of physiological air-water interfaces for therapeutic purposes is challenging because it is difficult to molecularly spread polymers on the water surface

without using an organic spreading solvent. 9,10 Recently, our group has demonstrated that water-spread monolayers of amphiphilic block copolymer micelles can have surface mechanical characteristics that closely mimic those of natural lung surfactant monolayers; aqueous micelles formed with poly(styrene-block-ethylene glycol) (PS-PEG) block copolymers spontaneously spread on the water surface (without undergoing any change in micellar morphology) and form an insoluble micelle monolayer that is capable of producing near-zero surface tension under high compression. 9,11 This micelle monolayer system bears a resemblance to polymer-brushed nanoparticle monolayers and differs from the conventionally

Received: June 9, 2023
Revised: August 25, 2023
Published: September 14, 2023





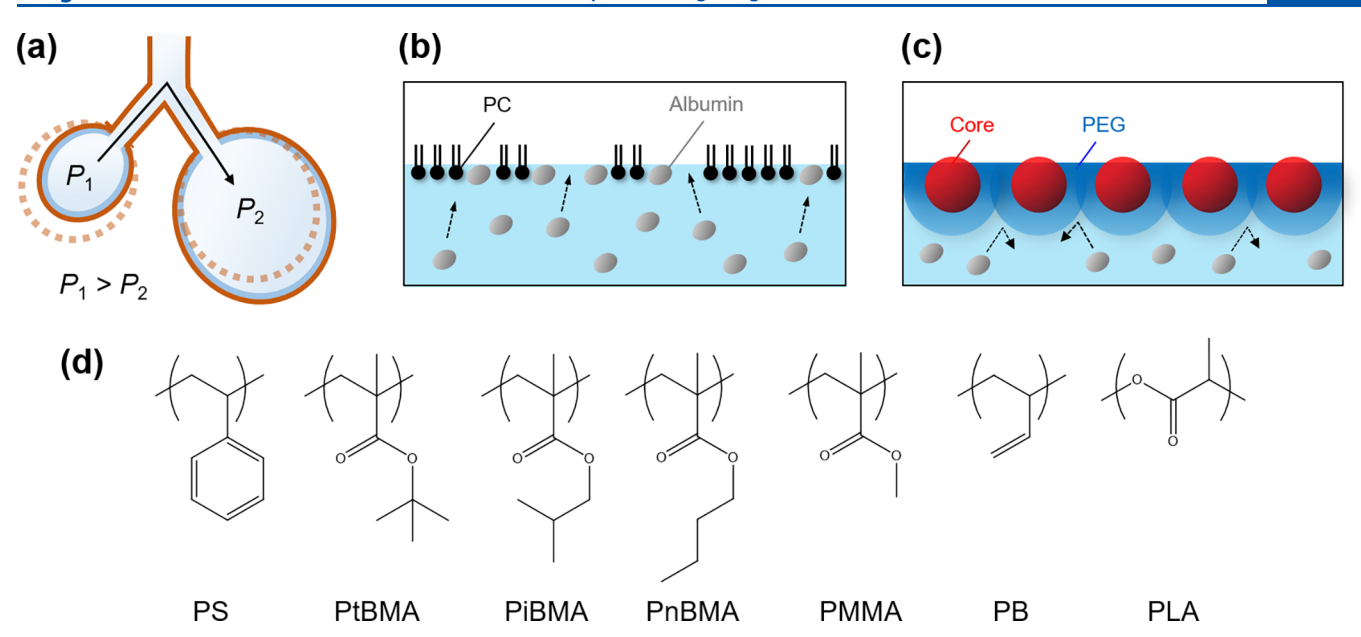


Figure 1. (a) Lung surfactant dysfunction causes the collapse of small alveoli due to an imbalance in the Laplace pressure. The displacement of the alveolar walls from the dotted to solid lines depicts the gradual collapse of the alveolar structure of the lung. (b) Replacement of lung surfactant lipids (such as phosphatidylcholine (PC)) with serum proteins (such as albumin) at the alveolar air—water interface is a cause of surfactant dysfunction in injured lungs. (c) Block copolymer micelles form stable monolayers on the surface of alveolar lining fluid that are resistant against protein adsorption. (d) Hydrophobic block chemistries examined in this study: poly(styrene) (PS), poly(t-butyl methacrylate) (PtBMA), poly(isobutyl methacrylate) (PiBMA), poly(n-butyl methacrylate) (PnBMA), poly(methyl methacrylate) (PMMA), poly(1,2-butadiene) (PB), and poly(p,L-lactic acid) (PLA).

studied block copolymer films. The latter are typically prepared by spreading the polymer from a state of singly dispersed chains using cosolvents, forming a continuous asymmetric monolayer or "surface micelles". 7,8 For clinical and therapeutic applications, it is imperative that polymers are administered in an aqueous suspension, precluding the use of organic solvents. This necessity drives the hydrophilic modification of the polymer, which is typically achieved through PEGylation. PEG-based amphiphilic block copolymers exhibit the propensity to assemble into micellar nanostructures within aqueous environments. Furthermore, unlike lipid-based lung surfactant compositions (such as the calf-derived Infasurf), this polymer lung surfactant (PLS) composed of PS-PEG micelles exhibits the advantage of evading the detrimental impact of biological inhibitors such as serum proteins and phospholipases under acute respiratory distress syndrome (ARDS) conditions. Serum proteins are known to competitively adsorb at the air-water interface within alveoli, functioning as inhibitors for lipid-based lung surfactants, whether natural or synthetic, during lung injury situations (as depicted in Figure 1). 5,12-14 Our previous research has demonstrated that PLS maintains its capability to lower surface tension (increase surface pressure (Π)), even in the presence of albumin, a model serum protein. 9,10 Moreover, PLS naturally remains unaffected by enzymatic degradation by phospholipases, which are activated under inflammation.² Given its commendable physiological behavior and economical feasibility for production scale-up, PLS holds substantial promise as an alternative to current lipid-based lung surfactants for treating conditions such as ARDS and related ailments.9

Previously, we have shown that changing the overall size of PS-PEG (while holding the PEG block size constant) significantly influences the surface mechanical properties of PS-PEG micelles⁹ and also that differently sized micelles prepared using an identical PS-PEG material behave differently

with one another at the air-water interface. 9,11 Herein, we extend these previous studies to other PEG-based block copolymers. Specifically, this study aims to investigate the effect of hydrophobic block chemistry on the surface mechanics of PEG-based copolymer micelles. The ultimate goal of these efforts is to establish design principles for block copolymer micelle-based PLS formulations for use as a surfactant replacement therapy for respiratory distress syndrome (including ARDS). To be suitable for this application, block copolymer micelles must be able to (i) reduce the air—water interfacial tension (γ) to close to zero at maximum compression (in order to minimize the work associated with expanding the alveolar surface area (A) at the onset of and during inhalation) and (ii) enhance the area compressibility modulus, $E = (A(\partial \gamma/\partial A) = -A(\partial \Pi/\partial A))$, of the alveolar air-water interface so that the alveolar tissues are stabilized against collapse due to a gradient in the Laplace pressure (Figure 1(a)). 13,15 By analogy to the fact that the hydrophilic-lipophilic balance and the fluidity of the hydrophobic tail group control the interfacial mechanics of lipids, 16 it is reasonable to expect that the surface mechanical properties of block copolymer micelles are also controlled by the hydrophobicity and the mechanical rigidity/deformability of the micelle core material. Similar observations have also been reported for colloidal particles at air-water and oil-water interfaces. 17,18

In this study, eight different PEG-based diblock copolymers having comparable molecular weights but different hydrophobic block chemistries (Figure 1(d)) were used. The water contact angle (θ) and glass-transition temperature ($T_{\rm g}$) properties of the hydrophobic block materials were characterized to quantify the thermodynamic affinity for the airwater interface and the compliance of the polymer micelles under lateral compression, respectively. Spherical micelles

Table 1. Molecular Characteristics of the Block Copolymers Studied^{a,b}

Polymer	PEG End Group	$M_{ m n,core} \ ({ m g/mol})^c$	$M_{\rm n,PEG} \ ({\rm g/mol})^d$	$M_{\rm w}/M_{\rm n}^{\ e}$	$\theta (\deg)^f$	$T_{\rm g}$ (°C) $^{\rm g}$
PS-PEG	-OCH ₃	5152	5000	1.23	88.8 ^h	85
PS-PEG-OH	-OH	5200	5500	1.11	88.8 ^h	86
PtBMA-PEG	-OCH ₃	6079	5000	1.19	85.8 ^h	94
PiBMA-PEG	-OCH ₃	5481	5000	1.23	87.8 ^h	51
PnBMA-PEG	-OCH ₃	7192	5000	1.11	83.2 ^h	16
PMMA-PEG	-OCH ₃	3739	5000	1.22	68.2 ^h	87
PB-PEG-OH	-OH	5000	4500	1.12	$96.0^{21,i}$	-3
PLA-PEG	-OCH ₃	3693	5000	1.47	$79.8^{22,i}$	35

 $^{a}M_{\rm n}$ is the overall number-average molecular weight of the block copolymer. $^{b}M_{\rm w}$ is the overall weight-average molecular weight of the block copolymer. $^{c}M_{\rm n,core}$ is the number-average molecular weight of the hydrophobic micelle core-forming block (determined by 1 H NMR). $^{d}M_{\rm n,PEG}$ is the number-average molecular weight of the hydrophilic micelle corona-forming PEG block (determined by 1 H NMR). $^{c}M_{\rm w}/M_{\rm n}$ is the overall molecular weight polydispersity index (determined by GPC). $^{f}\theta$ is the water advancing contact angle of the hydrophobic block (measured using spin-cast films of hydrophobic homopolymers having the same respective molecular weights as the hydrophobic blocks of the block copolymers). $^{g}T_{\rm g}$ is the glass-transition temperature of the hydrophobic block (values estimated for the corresponding hydrophobic homopolymers in the bulk state at the respective specific molecular weights using the Flory—Fox relation and our own DSC and literature $T_{\rm g}$ data). h Measurements were performed in this study. h Values were taken from the literature.

having comparable size characteristics were prepared from these copolymers by equilibration-nanoprecipitation (ENP). 9,11 Aqueous micelle suspensions were spread onto clean water subphases in a Langmuir trough to form micelle monolayers. Simultaneous surface pressure-area isotherm and Brewster angle microscopy (BAM) imaging/reflectivity measurements were performed on these water-spread micelle monolayers over varying surface areas in order to understand how the monolayer's structure and mechanical properties evolve during compression and also how the structural and mechanical attributes are interrelated to each other. From these data, structural behaviors responsible for diverse mechanical responses of the micelle monolayers under compression could be deduced, including deformation and even coalescence of the micelle cores, desorption of the micelles from the interface, and wrinkling and collapse of the monolayer. We also found strong correlations between the surface pressure-area isotherm pattern of the monolayer and the θ and T_g properties of the hydrophobic block polymer by multivariate correlation analysis. Based on these results, guiding principles can be used to search for and design candidate PLS therapeutics for ARDS that can benefit millions of patients worldwide. 19,20

RESULTS AND DISCUSSION

Preparation and Characterization of Block Copolymers and Block Copolymer Micelles. Table 1 lists the molecular characteristics of poly(ethylene glycol) (PEG)-based amphiphilic block copolymers used in this study. Diblock copolymers with low polydispersity indices ($M_{\rm w}/M_{\rm n}=1.1-1.5$, where $M_{\rm w}$ and $M_{\rm n}$ denote the weight- and number-average overall molecular weights of the block copolymer, respectively) were prepared by controlled polymerization techniques (Figures S1-S6 in the Supporting Information (SI)). Since the surface mechanical properties of block copolymer micelles depend on the molecular weight of the block copolymer, we tried to keep the molecular weights of the diblock copolymers within a relatively narrow range (8.7–13.8 kDa); the target molecular weight was 5 kDa for both the hydrophilic (PEG) and hydrophobic blocks. Hereafter, all block copolymers are named using the notation P(X)-PEG in which P(X) is the abbreviation for the hydrophobic block polymer, as listed in Figure 1(d). Except for the PS-PEG-OH and PB-PEG-OH

copolymers that have a hydroxyl group (-OH) at the end of the PEG block, all of the other block copolymers used have methoxy(-OCH₃)-ended PEG blocks.

Our hypothesis for this study is that the hydrophobicity and mechanical rigidity of the micelle core domain significantly influence the surface mechanical properties of polymer micelles. The hydrophobicity and rigidity can be measured, respectively, in terms of the wettability at the air-water interface and the bulk-state glass transition temperature (T_g) of the hydrophobic block polymer. The wettability (w) is defined as $w \equiv \gamma_{PW} - \gamma_{PA}$, where γ_{PW} and γ_{PA} are the polymer–water and polymer-air interfacial tensions, respectively, and is a measure of the thermodynamic tendency of the micelle core material to wet (i.e., anchor to) the air-water interface. The wettability can be measured by measuring the contact angle (θ) of a water droplet on a polymer substrate at the threephase (air-water-polymer) contact line; note according to Young's equation that $\gamma_{PA} = \gamma_{PW} + \gamma_{AW} \cos(\theta)$ where γ_{AW} is the air—water interfacial tension (= 72 mN/m at 25 °C)²³ and w $(\equiv \gamma_{\rm PW} - \gamma_{\rm PA}) = -\gamma_{\rm AW} \cos(\theta) \propto - \cos(\theta)$. For an accurate experimental determination of the θ (and T_g) properties of the hydrophobic blocks of the block copolymers studied, the corresponding homopolymers (having comparable molecular weights (6.6-8.2 kDa) were prepared; the molecular characteristics of the homopolymers used are summarized in Table S1.

Water contact angle (θ) and differential scanning calorimetry (DSC) measurements were performed on these homopolymers; the results are presented in Table 1, Table S1, and Figures S16 and S17 of the SI. In terms of their mechanical rigidity, the seven different hydrophobic block polymers studied can be divided into two groups: rigid polymers with $T_g > 60$ °C (PS, PtBMA, and PMMA in the bulk state) vs soft polymers with $T_{\rm g}$ < 60 °C (PB, PiBMA, PnBMA, and PLA in the bulk state). Note that the use of 60 °C as the boundary for defining rigid vs soft polymers is arbitrary and for convenience. Also, the actual T_{σ} of a polymer in the micelle form can be different from when it is in the bulk state because the glass-transition behavior can be influenced by the (micellar) nanoconfinement,²⁴ the plasticizing effect of water,²⁵ and the localization of the block junction points.²⁶ A study is currently in progress in our laboratory to accurately determine the T_g properties of polymer micelles using techniques such as transverse proton NMR relaxation and

Table 2. Structural and Surface Mechanical Properties of the Block Copolymer Micelles

Polymer	$arphi_{ ext{w,ENP}}^{a}$	$D_{\rm c} ({\rm nm})^{b}$	$D_{ m h} \ (m nm)^c$	$\mathrm{PDI}_{\mathrm{DLS}}^{}}^{}}}}$	$\sigma_{ ext{PEG}}^{e}$	$E_{\rm max} ({\rm mN/m})^f$	Π at $E_{\rm max}~({\rm mN/m})^{\rm g}$	$\Pi_{\rm max} \left({\rm mN/m}\right)^{h}$
PS-PEG	0.1	19.0	31.4	0.157	9.71	184.7	40.8	63.5
PS-PEG-OH	0.5	16.5	31.2	0.082	9.37	99.8	62.1	69.4
PtBMA-PEG	0.3	17.1	27.5	0.082	7.21	133.1	55.1	67.7
PiBMA-PEG	0.1	17.1	28.6	0.018	8.19	117.4	50.7	64.2
PnBMA-PEG	0.3	16.9	26.1	0.012	6.26	60.5	53.0	60.7
PMMA-PEG	0.5	15.6	30.7	0.072	12.38	56.8	37.7	37.7
PB-PEG-OH	0.1	19.5 ⁱ	34.5	0.142	8.00	34.5	15.8	30.1
PLA-PEG	0.2	15.6	26.6	0.190	13.14	7.6	17.0	18.1

 $^a\varphi_{\rm w,ENP}$ is the volume fraction of water in the water/organic cosolvent (acetone) mixture in which equilibrium block copolymer micelles were initially formed during the equilibration—nanoprecipitation (ENP) formulation process. bD_c is the mean diameter of the hydrophobic core domains of the block copolymer micelles (determined by dry-state TEM). cD_h is the mean hydrodynamic diameter of the block copolymer micelles measured at a concentration of 0.05 wt % in Milli-Q water (determined by DLS/cumulant analysis). $^dPDI_{DLS}$ is the micelle size polydispersity index (determined by DLS/cumulant analysis). $^e\sigma_{\rm PEG}$ is the dimensionless PEG corona chain grafting density. $^fE_{\rm max}$ is the maximum compressibility modulus of the water-spread block copolymer micelle monolayer. $^g\Pi$ at $E_{\rm max}$ denotes the micelle monolayer surface pressure at maximum compressibility modulus. $^h\Pi_{\rm max}$ is the maximum surface pressure, which, in most cases, is equal to the surface pressure at monolayer collapse. i Corecross-linked PB-PEG-OH micelles were used for dry-state TEM analysis.

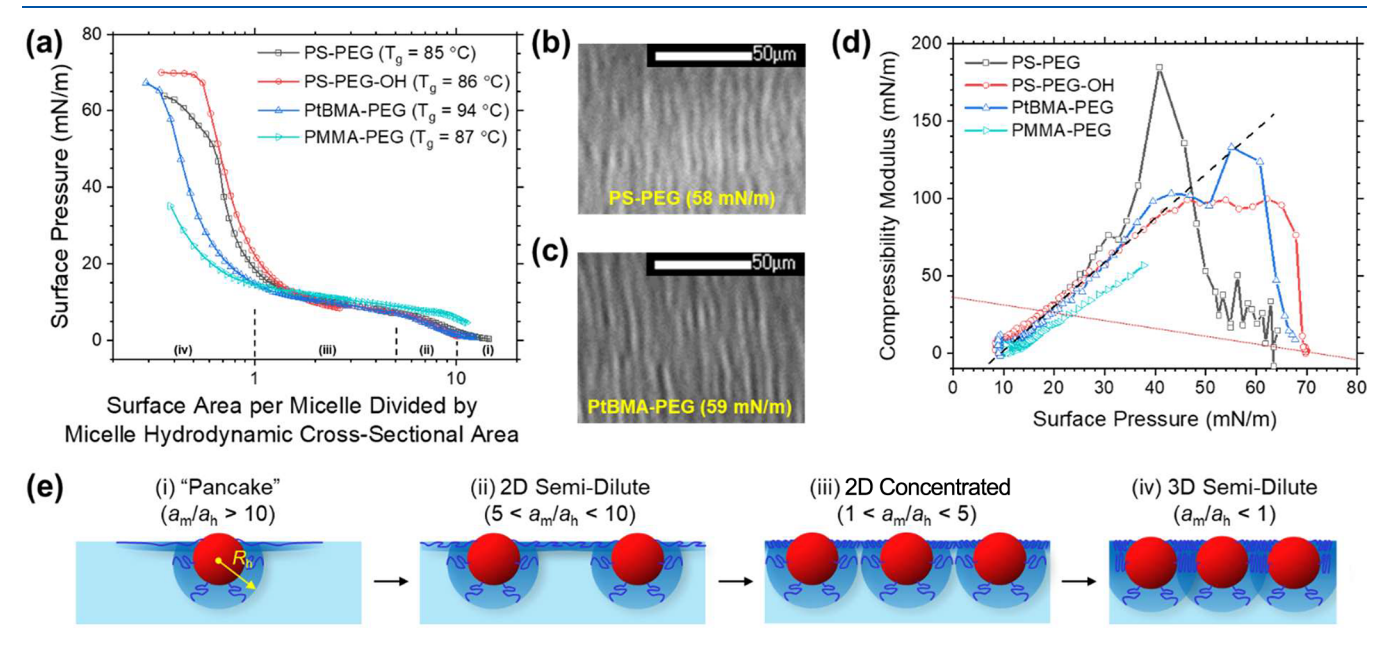


Figure 2. Surface mechanical behaviors of rigid core micelles ($T_{\rm g} > 60~{\rm ^{\circ}C}$). (a) Surface pressure (Π) vs surface area per micelle ($a_{\rm m}$) divided by the micelle hydrodynamic cross-sectional area ($a_{\rm h} = \pi R_{\rm h}^{-2}$) isotherms. Each isotherm curve represents a superposition of two data sets obtained by spreading 10 and 100 μ L of a 5 mg/mL block copolymer micelle solution in water onto a clean water surface at an initial surface area of 782 cm², respectively, and then by compressing the monolayer at a speed of 3 mm/min to a final area of 71 cm². The phase regions, as numbered in (e), have been indicated to correspond to various states of surface coverage. (b, c) Representative BAM images of PS-PEG and PtBMA-PEG micelle monolayers at high compression. The surface pressure (Π) values at which the BAM images were taken are given in parentheses. (d) Compressibility moduli (E) as functions of Π . The black dashed line is a linear fit to the data, and the slope of this line (y) is estimated to be 2.85. The red dotted line shows the limit of Laplace stability for the alveoli ($2E - \gamma > 0$). (e) Conformational changes in adsorbed PS-PEG micelles during compression.

molecular-rotor optical viscometry measurements. In the present study, using the bulk $T_{\rm g}$ values was sufficient for the purpose of testing for a correlation between the glass transition vs surface mechanical properties of block copolymer micelles. In terms of their degrees of hydrophobicity/wettability, the hydrophobic block polymers can be divided into two groups: more hydrophobic materials having $\theta > 80^{\circ}$ (PS, PtBMA, PiBMA, PnBMA, and PB) vs less hydrophobic materials having $\theta < 80^{\circ}$ (PMMA and PLA).

Micelles were prepared from the eight different block copolymers in water using the two-step equilibration—nanoprecipitation (ENP) method¹¹ and characterized by TEM and dynamic light scattering (DLS) (Table 2). All

micelles were spherical in shape, and their sizes were comparable within a narrow range across different block copolymers, i.e., $D_{\rm c}$ (core diameter determined by TEM) = 18 \pm 2 nm (Figure S18) and $D_{\rm h}$ (micelle hydrodynamic diameter by DLS) = 30 \pm 4 nm. The micelle structures were stabilized by dense PEG coronas which produce steric repulsion between the micelles and thus prevent them from aggregating and/or coalescing. As presented in Table 2, the dimensionless PEG grafting density values were much greater than 1 in all cases ($\sigma_{\rm PEG}$ = 6–13). Here, the dimensionless grafting density ($\sigma_{\rm PEG}$) is defined as $\sigma_{\rm PEG} \equiv pR_{\rm g,PEG}^2/D_{\rm c}^2$, that is, as the ratio of the projected cross-sectional area of a PEG chain in its unperturbed conformation ($\pi R_{\rm g,PEG}^2$) relative to the area per

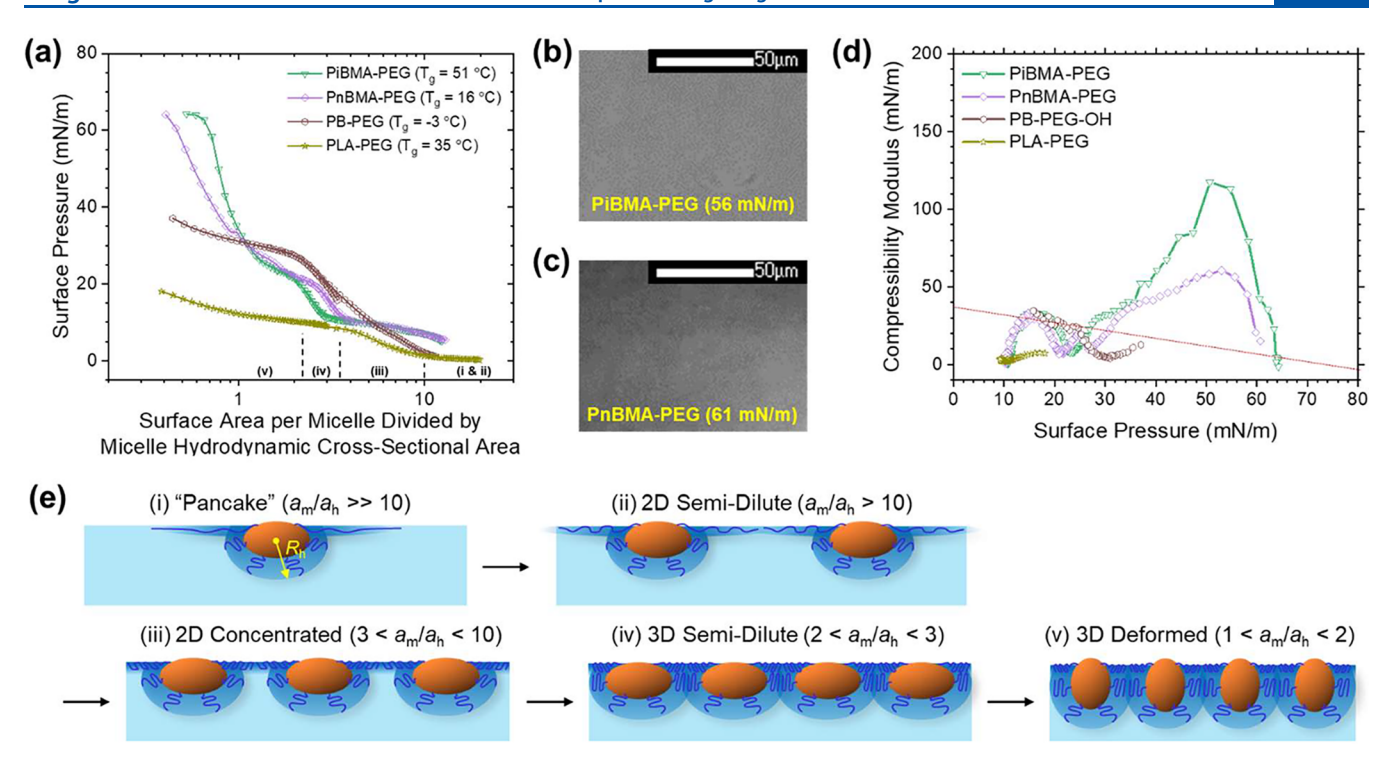


Figure 3. Surface mechanical behaviors of soft core micelles ($T_{\rm g}$ < 60 °C). (a) Surface pressure (Π) vs surface area per micelle ($a_{\rm m}$) divided by micelle hydrodynamic cross-sectional area ($a_{\rm h} = \pi R_{\rm h}^{-2}$) isotherms. Each isotherm curve represents a superposition of two data sets obtained by spreading 10 and 100 μ L of a 5 mg/mL block copolymer micelle solution in water onto a clean water surface at an initial surface area of 782 cm², respectively, and then by compressing the monolayer at a speed of 3 mm/min to a final area of 71 cm². The phase regions, as numbered in (e), have been indicated to correspond to various states of surface coverage. (b, c) Representative BAM images of PiBMA-PEG and PnBMA-PEG micelle monolayers at high compression. The surface pressure (Π) values at which the BAM images were taken are given in parentheses. (d) Compressibility moduli (E) as functions of Π. The red dotted line shows the limit of Laplace stability for the alveoli (2E – γ > 0). (e) Conformational changes in adsorbed PiBMA-PEG micelles during compression.

PEG corona chain at the micelle core surface $(\pi D_c^2/p)$, where $R_{\rm g,PEG}$ is the radius of gyration of the PEG block in the Gaussian state, $p = (\pi D_c^3/6)(M_{\rm n,core}/N_{\rm A}\rho_{\rm core})^{-1})$ is the aggregation number of the micelles, $M_{\rm n,core}$ is the numberaverage molecular weight of the hydrophobic (core-forming) block, $N_{\rm A}$ is Avogadro's number, and $\rho_{\rm core}$ is the mass density of the micelle core.

Surface Mechanics of Water-Spread Block Copolymer **Micelles.** Surface pressure—area $(\Pi - A)$ isotherms were determined for the block copolymer micelles after spreading them in the form of an aqueous solution onto the air-water interface within a Langmuir trough filled with Milli-Q water through compression of the surface at a rate of 4.5 cm²/min (equivalent to a linear speed of 3 mm/min). Here, the surface pressure (Π) is defined as the difference between the surface tension of the clean air-water interface (γ_0) and that of the micelle-laden air—water interface (γ) , that is, $\Pi \equiv \gamma_o - \gamma$. The surface area per micelle (a_m) was calculated as $a_m = A/N$, where A is the total surface area, $N = cVN_A/pM_n$ is the total number of micelles spread, c = 5 mg/mL is the concentration of the polymer (micelles) in the spreading solution, and V is the volume of the micelle solution spread. Because the surface area of the trough can be changed only by a factor of 11 (782 cm² \leftrightarrow 71 cm²) in an experiment, for each sample, $\Pi - a_{\rm m}$ isotherm measurements were performed twice using two different spreading volumes (V = 10 and $100 \mu L$) in order to cover a sufficient range of $a_{\rm m}$. In all cases, when 10 μL of the spreading solution was spread, the initial surface pressure of the micelles ($\Pi = 0-5 \text{ mN/m}$) was much lower than the

equilibrium spreading pressure of PEG ($\Pi_e \cong 10 \text{ mN/m}$). In this low surface concentration limit, it is reasonable to assume that the micelles spontaneously spread (due to the Marangoni effect) with negligible loss to the subphase (due to the strong affinity of PEG chains for the air—water interface^{28,29}). However, if the surface is already saturated with polymer micelles, then the surplus number of micelles would be submerged in the subphase during the spreading process; in this case, the true value of N is unknown but is expected to be smaller than that estimated based on stoichiometry.

For this reason, each $\Pi - a_{\rm m}$ isotherm curve obtained at V =100 μ L was horizontally shifted to match the reference Π – $a_{\rm m}$ isotherm obtained at $V = 10 \mu L$ by multiplying the a_m values by a constant shift factor (Figure S19). This superposition is justifiable based on two underlying assumptions: (i) that the equilibrium surface pressure (Π_{eq}) is a unique function of the surface area and (ii) that the recorded Π values from area scans represent values at or near equilibrium. This equivalence was validated through our observation, wherein Π exhibited minimal variation not exceeding 0.1 mN/m within a 40 min time frame when the area was maintained under the condition of $\Pi = 10-20$ mN/m (a range commonly associated with the superposition process). The combined (superposed) isotherms were further transformed into the final forms presented in Figures 2(a) and 3(a) by normalizing a_m by the hydrodynamic cross-sectional area of the micelles $(a_h = \pi D_h^2/4)$; during compression, the neighboring micelles start experiencing steric repulsive forces when $a_{\rm m}/a_{\rm h} \approx 1$. Additionally, $\Pi - a_{\rm m}$ isotherms capturing the full compression and expansion cycles

were acquired at an accelerated rate of 45 cm²/min (equivalent to a linear speed of 30 mm/min), concurrent with the BAM experiment (displayed in Figure S20). Significant hysteresis was observable across a majority of the samples, with particularly notable instances in monolayers consisting of PS-PEG-OH, PtBMA-PEG, and PiBMA-PEG micelles. These specific monolayers have been compressed beyond their respective collapse pressures. As such, the underlying cause of this phenomenon is linked to the desorption of micelles from the interface. This desorption encompasses monolayer collapse, folding, and/or potentially irreversible micelle loss to the subphase, all transpiring at the collapse pressure threshold. The gradual kinetics associated with the respreading of collapsed monolayers and/or the readsorption of desorbed micelles during the expansion process contributes to this behavior. A comprehensive analysis of these effects can be found in our earlier study pertaining to PS-PEG micelles of varying sizes.1

Micelles with Rigid (Glassy) Cores. Figure 2(a) displays the $\Pi - a_{\rm m}/a_{\rm h}$ isotherms for block copolymer micelles with rigid (glassy) cores at room temperature (with $T_{\rm g} > 60~^{\circ}{\rm C}$ in the bulk state); $T_g \cong 85-86$ °C and $\theta \cong 89$ ° for bulk PS, and $T_{\rm g}\cong 94$ °C and $\theta\cong 86^{\circ}$ for bulk PtBMA. The polymer micelles in this category showed a common pattern of surface pressure behavior. As schematically depicted in Figure 2(e), in the dilute micelle surface concentration limit, each isolated individual micelle is nearly fully immersed in water while at the same time it is strongly anchored to the air-water interface (data supporting this are presented/discussed throughout this subsection) because a significant number of the PEG corona chains are adsorbed and assume a two-dimensional (2D) flattened coil structure at the air-water interface; this PEG surface layer ("pancake") formation is driven by the strong affinity of PEG to the air-water interface.²⁸ As shown in Figure 2(a), when a_m/a_h reaches a value of about 10 during compression, the PEG pancakes (i.e., the adsorbed PEG chains) from different micelles start sterically interacting with each other, forming a 2D semidilute PEG solution, and as a result, Π starts rising faster than the ideal gas-like law predicts $(\Pi \sim A^{-1})$. In this 2D semidilute PEG surface concentration regime (i.e., at $5 < a_m/a_h < 10$), we found that Π actually scales with A to the power of approximately -4.9 (Figure S21). The de Gennes scaling theory predicts that in the semidilute concentration regime the osmotic pressure of a polymer solution (Π_{osm}) scales with the mass concentration of the polymer (c), i.e., $\Pi_{\text{osm}} \sim c^y$, and the scaling exponent, y, is related to the so-called Flory exponent, ν , by the equation y = $d\nu/(d\nu-1)$, where d is the dimensionality.³⁰ Applying this relation to our 2D situation (that is, $\Pi = \Pi_{\text{osm}}$, d = 2, and $c \sim A^{-1}$) gives $\Pi \sim A^{-y}$, where $y = 2\nu/(2\nu - 1)$.^{4,5,31} Therefore, the 2D Flory exponent for the adsorbed PEG corona chains is estimated to be $\nu \cong 0.63$, which suggests that the air-water interface provides a "good solvent" environment for the PEG chains, 32 and thus the adsorbed PEG chains are expected to assume extended conformations in the 2D space. 33 Note, however, that this 2D Flory exponent of the micellar PEG chains is lower than that previously reported for free PEG chains at the air—water interface ($\nu \cong 0.77$).

Further compression leads to a plateau in Π at $a_{\rm m}/a_{\rm h}\approx 5$. The plateau surface pressure coincides with the equilibrium spreading pressure of PEG ($\Pi_{\rm e,PEG}\cong 10~{\rm mN/m}$),³⁴ which suggests that at the plateau transition the air—water interface becomes fully saturated with the adsorbed PEG chains. Within

the plateau region (1 < $a_{\rm m}/a_{\rm h}$ < 5), continued compression causes a gradual desorption of the adsorbed PEG segments into the subphase, while the water surface remains saturated with the remaining adsorbed PEG segments, which causes the surface pressure to remain constant.

When the micelle monolayer is compressed beyond $a_{\rm m}/a_{\rm h} \approx$ 1, as depicted in Figure 2(e), the nonadsorbed PEG corona chains in the subphase overlap with each other between neighboring micelles, which leads to an even faster rise in Π with compression. As further discussed below (with reference to Figure 2(b)), this surface pressure rise is, again, believed to be due to a buildup of the semidilute PEG osmotic pressure (Π_{osm}) ; in this case, the osmotic pressure is built up, not within the PEG pancake layer but in the subphase region. Previously, on the basis of the analysis of Brewster angle microscopy (BAM) images, we have estimated that in PS-PEG micelle monolayers the compressive stress applied to the monolayer during compression is stored within a layer of about 1 nm thickness. 11 This "mechanical" thickness (t_m) was estimated using a model adapted from lipid fluid membranes: $t_{\rm m} = (\beta B/$ $(E)^{1/2}$, where B is the bending stiffness of the monolayer, derived as $B = (\Delta \rho) g \lambda^4 / (16\pi^4)$, incorporates parameters such as the wrinkle wavelength (λ) , the density difference between air and water $(\Delta \rho)$, the gravitational constant (g), and the compressibility modulus (E). This stress-bearing layer exhibited a thinner profile compared to the overall thickness of the micelle monolayers. This phenomenon can be attributed to the high curvature of the micelle core surface, as the area of corona overlap between adjacent micelles remains relatively diminutive (~5 nm in cross-sectional diameter at maximum overlap, as depicted in Figure 2(e)). In this semidilute PEG subphase concentration regime (i.e., at $a_{\rm m}/a_{\rm h}$ < 1), the unrelaxed osmotic pressure produced by compression causes the micelle monolayer to form wrinkles and eventually to collapse and fold, as can be seen in BAM images in Figure 2(b) and 2(c). In all cases involving micelles with rigid and strongly hydrophobic cores (i.e., PS-PEG, PS-PEG-OH, and PtBMA-PEG micelles), wrinkles appeared in the micelle monolayers when the compression exceeded their respective maximum compressibility modulus values (E_{max}). Detailed characteristics of the wrinkled structures have been discussed in our previous publication. 11 In each of these three cases, the maximum surface pressure, $\Pi_{\rm max}$ was approximately 70 mN/m (the surface tension was nearly zero at maximum compression; Table 2). These results suggest that these PS-PEG, PS-PEG-OH, and PtBMA-PEG micelles have an extremely strong affinity for the air-water interface due to the strong hydrophobic character of the core-forming blocks, and as a result, the micelle monolayers were able to withstand the lateral compression without losing material to the subphase. On the contrary, as shown in Figure 2(a), micelles with (rigid but) less hydrophobic cores (i.e., PMMA-PEG micelles) failed to resist the compression and were unable to produce sufficiently high surface pressure; no wrinkles were observed in this system.

The lower area portions of the $\Pi-a_{\rm m}/a_{\rm h}$ isotherms shown in Figure 2(a) were further converted to plots of E vs Π (Figure 2(d)). As shown in Figure 2(d), in the intermediate- Π regime (i.e., at $\Pi \cong 10-30$ mN/m), the $E-\Pi$ curves for PS-PEG, PS-PEG-OH, and PtBMA-PEG micelles were found to superimpose into a single straight line, which is consistent with the prediction of the semidilute scaling theory. As discussed earlier, since $\Pi - \Pi_{\rm e,PEG} = \Pi_{\rm osm} \sim c^y \sim A^{-y}$ (where $y = {\rm d}\nu/({\rm d}\nu - 1)$),

 $E \ (\equiv -A(\partial \Pi/\partial A) = -A(\partial \Pi_{\text{osm}}/\partial A)) = y\Pi_{\text{osm}} = y\Pi$ $y\Pi_{e,PEG}$ (const.). The slope of the $E-\Pi$ lines was estimated to be $y = 2.85 \pm 0.05$; the exact same behavior (y = 2.8 - 2.9) has previously been observed for PS-PEG micelles having different core diameters ($D_c = 14-27$ nm) (see Figure 4(C) of ref 11). As discussed above, in this regime, Π increases during compression due to an overlap of the subphase PEG corona layers between adjacent micelles; therefore, d = 3 (i.e., the overlap occurs in 3D space). From the value of the slope (y =2.85), therefore, the value of the 3D Flory exponent for the PEG corona chains could be determined ($\nu \cong 0.51$). We note that this ν value is lower than that reported for free PEG chains in water $(\nu \cong 0.58)^{.35}$ but this result is consistent with our previous observation that PEG chains experience a closer to poor-solvent environment when they exist in the end-grafted (brush) state. 36,37

Interestingly, as shown in Figure 2(d), in the case of PMMA-PEG micelles ($T_{\rm g}\cong 87\,^{\circ}{\rm C}$ and $\theta\cong 68^{\circ}$ for bulk PMPMA), the slope (y) of the E vs Π graph was equal to 2.85 only within a narrow range of Π (= 15–20 mN/m) but decreased to a lower value (y=1.49) at $\Pi>20$ mN/m due to continuous desorption of the micelles from the air—water interface; the desorption of PMMA-PEG micelles is thought to be due to the relatively less hydrophobic nature of PMMA and is further supported by quantitative Brewster angle microscopy (QBAM) analysis (discussed later).

Micelles with Soft Cores. As shown in Figure 3(a), the $\Pi - a_{\rm m}/a_{\rm h}$ isotherms for soft core micelles ($T_{\rm g}$ < 60 °C) did not follow the general overall trends observed with the rigid core micelles. The monolayers of PiBMA-PEG and PnBMA-PEG micelles (having soft and strongly hydrophobic cores) exhibited the PEG desorption plateau ($\Pi_{e,PEG}$) at higher surface areas $(a_{\rm m}/a_{\rm h} \approx 4{-}10)$ than those for the rigid core micelles $(a_{\rm m}/a_{\rm h}=2-5)$; note that $T_{\rm g}\cong 51~{\rm ^{\circ}C}$ and $\theta\cong 89^{\rm ^{\circ}}$ for bulk PiBMA and $T_{\rm g}\cong 16~^{\circ}{\rm C}$ and $\check{\theta}\cong 83^{\circ}$ for bulk PnBMA. Further compression caused a rapid upturn in Π followed by a second plateau. The onset of the upturn (corona overlap between micelles) occurred at $a_{\rm m}/a_{\rm h} > 1$, which indicates that the soft core micelles had a flattened (oblate) shape at the airwater interface (further supported by QBAM analysis, discussed later) in order to maximize the contact between the hydrophobic core and the air (Figure 3(e)); similar behavior has been reported for soft microgels. 38,39 The second plateau, we believe, is due to the deformation (vertical elongation) of the core domains (also supported by QBAM, discussed later). Micelle fusion, however, did not seem to occur because further compression caused an increase in Π beyond 60 mN/m. At $a_{\rm m}/a_{\rm h}$ < 1, these micelles produced

reasonably high surface pressures ($\Pi_{max} > 60 \text{ mN/m}$) and showed indications of monolayer collapse (the high-pressure plateau) similar to the micelles having rigid and strongly hydrophobic cores (such as PS-PEG micelles). However, no wrinkles were observed for all surface areas examined (Figure 3(b) and 3(c)), which suggests that the compressive stress was relaxed by core deformation in this case (rather than by the formation of wrinkles). Hence, the occurrence or absence of wrinkling under high compression provides a discriminative criterion between "rigid monolayers", characterized by micelles such as PS-PEG and PtBMA-PEG, and "soft monolayers", encompassing micelles such as PiBMA-PEG and PnBMA-PEG. Notably, the rigid monolayers exhibit a more pronounced increase in Π along surface pressure—area isotherms and generally higher values of $E_{
m max}$. We note that the $T_{
m g}$ of the micelle core is in general much lower than the $T_{\rm g}$ of the polymer in the bulk state (bulk $T_{\rm g}$ data presented in Table 1).²⁴ On the basis of the surface mechanical behavior of the PiBMA-PEG micelles, for instance, it is reasonable to expect that the T_{σ} of the PiBMA core is lower than room temperature. Unfortunately, however, precise experimental determination of the micelle core T_g remains a difficult task.^{40,41}

PB-PEG-OH micelles have a strongly hydrophobic but liquid-like core ($\theta \cong 96^{\circ}$ and $T_{\rm g} \cong -3 \, {\rm ^{\circ}C}$ for bulk PB). The surface pressure-area isotherm of water-spread PB-PEG-OH micelles was identical to that reported for a chloroform-spread PB-PEG-OH monolayer. 42 As shown in Figure 3(a), in this PB-PEG-OH case, the PEG plateau $(\Pi_{e,PEG})$ almost did not occur; there was only a slight shoulder in the isotherm curve at $a_{\rm m}/a_{\rm h}\cong 7.$ Instead, Π steadily increased until it reached a plateau at $\Pi \cong 30 \text{ mN/m} \ (>\Pi_{\text{e,PEG}})$ at $a_{\text{m}}/a_{\text{h}} \cong 2$. This plateauing indicates that PB-PEG-OH micelles merged into a continuous layer, which was enabled due to the liquid-like nature of the PB domain and also the strong tendency of PB to wet the air-water interface; 43 the spreading coefficient of PB ($s \ (\equiv \gamma_{\rm AW} - \gamma_{\rm PA} - \gamma_{\rm PW}) = 14 \ {\rm mN/m})$ is positive at room temperature. 44,45 Further compression caused a gradual slight increase in Π (at $a_{\rm m}/a_{\rm h}\lesssim 2$), which is likely due to a viscoelastic effect.

PLA-PEG micelles having soft and less hydrophobic cores exhibited a plateau at $\Pi_{\rm e,PEG}$ (Figure 3(a)); note that $T_{\rm g}\cong 35$ °C and $\theta\cong 80$ ° for bulk PLA. However, for this group, further compression caused only a slight increase in Π . Similar to the PMMA-PEG micelles (having a rigid but less hydrophobic core), Π did not become saturated, even at maximum compression (at $a_{\rm m}/a_{\rm h}\approx 0.4$). These results suggest that, at $\Pi>\Pi_{\rm e,PEG}$, the polymer micelles continuously desorbed from the air—water interface during compression, which prohibited a buildup of osmotic pressure. Similar behavior has also been reported for poly(lactic acid-co-glycolic acid)-b-PEG (PLGA-PEG) micelles.

As shown in Figure 3(d), the E vs Π curves were more complicated for the polymer micelles having softer cores because of the occurrence of an intermediate plateau at $\Pi > \Pi_{e,PEG}$. There was a clear trend in the E_{max} data for the micelles having soft and strongly hydrophobic cores; E_{max} decreased with decreasing T_g (i.e., PiBMA-PEG > PnBMA-PEG > PB-PEG-OH), which indicates that the micelle core rigidity controls the E of the micelle monolayer. The PiBMA-PEG and PnBMA-PEG micelles (having highly hydrophobic cores) were still able to produce $\Pi_{max} > 60$ mN/m, which suggests that these micelles did not become desorbed from the air—water interface even under high lateral compression nor did they

merge and transform into a continuous film (because of the metastability of the micelle structure, although both of these polymers have positive spreading coefficients, i.e., $s \cong 13 \text{ mN/m}$ for PiBMA²¹ and $s \cong 18 \text{ mN/m}$ for PnBMA²¹). The PLA-PEG micelles (having less hydrophobic cores) were characterized by relatively very small values of E_{max} (<10 mN/m) because of the micelle desorption. The values of E_{max} , Π at E_{max} and Π_{max} for all polymers tested are summarized in Table 2.

Table 3. Coefficients of Determination (R^2) for the Oneand Two-Dimensional Linear Regression of the Surface Mechanical Properties of the Block Copolymer Micelles $(E_{\text{max}}, \Pi \text{ at } E_{\text{peak}}, \text{ and } \Pi_{\text{max}})$ as Functions of Their Physicochemical Characteristics (T_g, θ)

		R^2				
Variable 1	Variable 2	$\begin{array}{c} \text{Maximum} \\ \text{Compressibility} \\ \text{Modulus} \ (E_{\text{max}}) \end{array}$	Surface Pressure (Π) at E_{\max}	$\begin{array}{c} \text{Maximum} \\ \text{Surface} \\ \text{Pressure} \\ \left(\Pi_{\text{max}}\right) \end{array}$		
T_{g}	_	0.415	0.312	0.256		
θ	_	0.079	0.000	0.077		
$T_{ m g}$	θ	0.707	0.356	0.492		

Bivariate Correlation Regression Analysis. The results presented in the previous subsections establish that the core rigidity and hydrophobicity (measured in terms of T_g and θ , respectively) determine the surface mechanics of the micelle monolayer. Previously, using PS-PEG micelles of systematically varying sizes (derived from an identical PS-PEG material), we have shown that the micelle core diameter (D_c) (which scales with the PEG corona chain grafting density $(\sigma_{ ext{PEG}}))$ is also an important factor that determines the surface mechanical properties of the micelles. 11 In the present work, we performed univariate and bivariate correlation regression analyses with measures of monolayer surface mechanics (E_{max} , Π at E_{peak} , and Π_{max}) as dependent variables and micelle physicochemical characteristics ($T_{\rm g}$ and θ) as independent variables. Table 3 summarizes the values of the coefficients of determination (R^2) obtained from these analyses. As shown in the table, the R^2 values from the univariate analysis were generally lower than those from the bivariate analysis, which suggests that the surface mechanical properties of polymer micelles are not controlled by a single parameter. Figure 4 displays 2D color maps of E_{max} , Π at E_{peak} , and Π_{max} as functions of $\{T_{g'}, \theta\}$, which graphically illustrate that E_{max} and Π_{max} show bivariate

correlations with $T_{\rm g}$ and θ . The values of $E_{\rm max}$, Π at $E_{\rm peak}$, and $\Pi_{\rm max}$ were highest in the upper right corner of the $T_{\rm g}-\theta$ plane (i.e., when both $T_{\rm g}$ and θ are greatest). These results support the idea that the micelle core $T_{\rm g}$ and θ are coupled parameters that simultaneously influence the micelle surface mechanics.

Quantitative Brewster Angle Microscopy (Reflectivity) Analysis. Quantitative Brewster angle microscopy (QBAM) analysis was performed to investigate how the structures of the micelle monolayers change during compression and how core $T_{\rm g}$ and θ influence the monolayer structure under compression. In QBAM experiments, the reflectivity of p-polarized light from the micelle-laden water surface at the Brewster angle of water (= 53.1°) was measured as a function of monolayer surface area. For a homogeneous film of thickness t and refractive index $n_{\rm f}$ on a water surface, the reflectivity (R) at the Brewster angle is given as

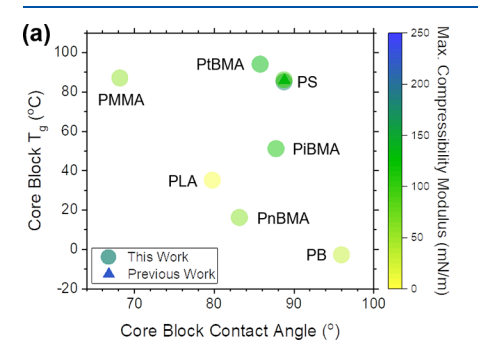
$$R = \left(\frac{\pi t}{\lambda}\right)^2 \left[\frac{n_{\rm f}^2 - n_{\rm w}^2 - 1 + (n_{\rm w}^2/n_{\rm f}^2)}{1 + n_{\rm w}^2}\right]^2 \tag{1}$$

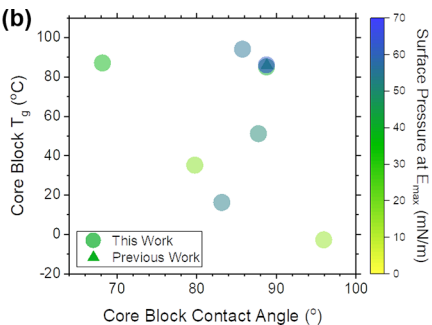
where λ is the wavelength of light and $n_{\rm w}$ is the refractive index of water. The refractive index of the film, $n_{\rm p}$ can be estimated using

$$n_{\rm f} \cong n_{\rm w} + \frac{{\rm d}n}{{\rm d}c} \frac{M}{At}$$
 (2)

where dn/dc is the specific refractive index increment, which can be estimated as $w_{\rm core}(dn/dc)_{\rm core} + w_{\rm corona}(dn/dc)_{\rm corona}$ (here, w_i and $(dn/dc)_i$ are, respectively, the weight fraction and specific refractive index increment of species i), M is the total mass of the micelles at the air—water interface, and A is the total area of the micelle monolayer. For insoluble (nondesorbing) monolayers formed by micelles having rigid (nondeformable) cores, it is expected that M and t are constant (unchanged) during compression. The values of R were computed from video recordings of BAM images. Representative BAM images and R vs A plots for all block copolymer micelles tested are presented in Figures S22–S30 of the SI.

Figure 5(a) shows both Π vs A and $R^{1/2}$ vs A plots (stacked on a shared x axis) for PS-PEG-OH micelles. The high-A (i.e., noncollapsed monolayer) portion of the $R^{1/2}$ vs A curve was first fit to eq 1 by using M and t as adjustable parameters; the actual quantity of polymer micelles at the air—water interface (M) is not known because of possible initial loss of micelles to the subphase during the spreading process. As shown with a dashed line in Figure 5(a), the reflectivity profile was well fit with a thickness value of t=8 nm at high to intermediate





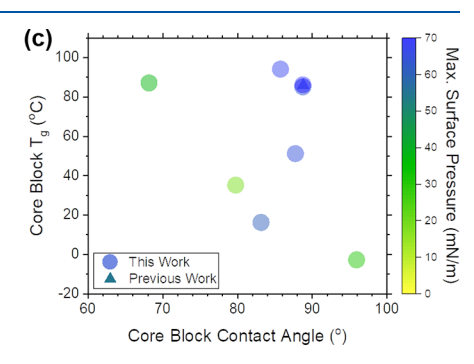


Figure 4. Two-dimensional plots of the (a) maximum compressibility modulus $(E_{\rm max})$, (b) surface pressure at $E_{\rm max}$ and (c) maximum surface pressure $(\Pi_{\rm max})$ as functions of the glass transition temperature $(T_{\rm g})$ and contact angle (θ) of the core-forming block. $E_{\rm max}$ Π at $E_{\rm peak}$ and $\Pi_{\rm max}$ data obtained in our previous study using PS-PEG-OH micelles are also displayed (triangles).

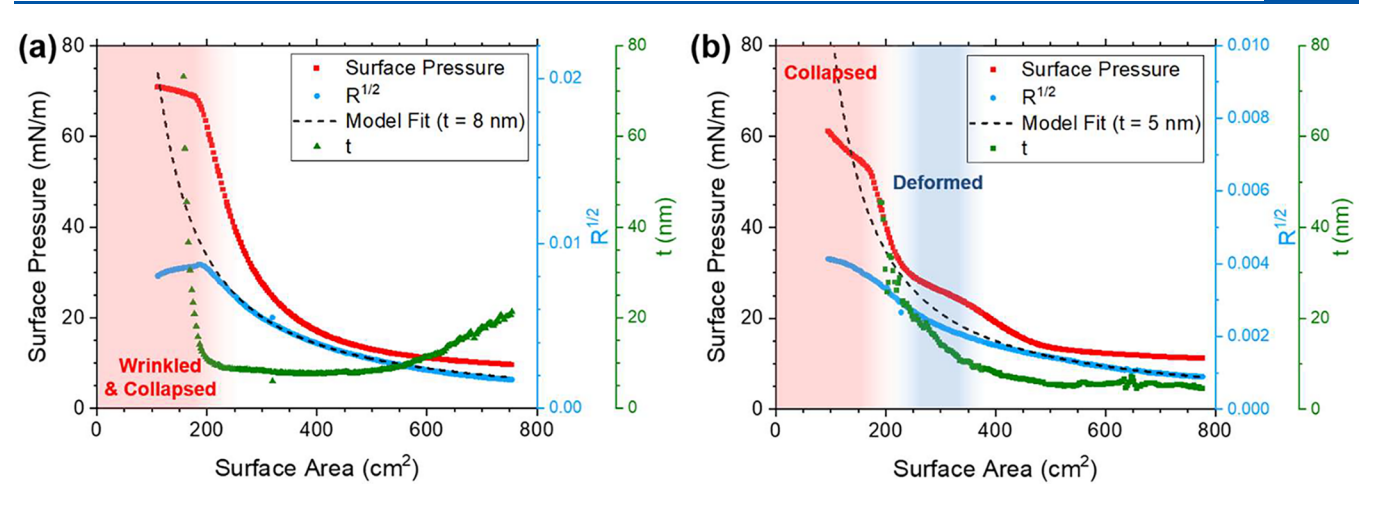


Figure 5. Surface pressure (Π , red squares) and square root of reflectivity at the Brewster angle ($R^{1/2}$, blue circles) measured as functions of surface area (A) during compression at a barrier speed of 30 mm/min after 100 μ L of a 5 mg/mL block copolymer micelle solution in water was spread onto a clean water surface at an initial surface area of 777 cm². The $R^{1/2}$ data were fit to eq 1 at a constant optical thickness (t) (dashed line). Alternatively, the values of t (green triangles) were also estimated from the $R^{1/2}$ data using eq 1. (a) The PS-PEG-OH micelle monolayer became wrinkled and collapsed at Π > 68 mN/m, which caused the deviation of the experimental R data from the prediction of eq 1 at constant t. The values of t calculated from the measured values of t using eq 1 were constant at t = 233–513 cm². (b) The PiBMA-PEG micelle monolayer showed a secondary plateau at t = 25–30 mN/m. The onset of the secondary plateau coincided with the onset of deviation of the experimental t from the model fit with constant t and also with the onset of the increase in t estimated from t.

surface areas ($A \cong 233-777 \text{ cm}^2$) (i.e., until Π reached Π_{max} during compression), which supports that PS-PEG-OH micelles are indeed nondesorbing even at reasonably high Π and the PS core does not deform under compression due to its high T_g . At high compression ($A \lesssim 200 \text{ cm}^2$), the constant-t model was no longer able to fit the data because of the formation of wrinkles and collapsed structures. We note that the best-fit thickness value (t = 8 nm) is smaller than the micelle core diameter ($D_c = 16.5$ nm) because the micelle monolayer is not a solid film; it contains interstitial regions between micelle cores, which are filled with water and PEG corona chains (Figure 2(e)). An alternative analysis was also performed in which t was calculated from measured R using eq 1 at constant *M* (determined by fitting as described above). As shown in Figure 5(a) (green triangles), t was found to be nearly constant over a wide range of surface areas ($A \cong 230$ -550 cm²). At A > 550 cm² (during the initial period of compression), t was overestimated, likely because of a small bias error in reflectivity calibration, of which the effect became negligible as the reflectivity signal was increased at higher compression. Compression past ~200 cm² caused a continuous increase in the estimated value of t because of wrinkling and collapse of the monolayer. As shown in Figures S22 and S24, PS-PEG and PtBMA-PEG micelles (having rigid and strongly hydrophobic cores) also exhibited similar reflectivity behaviors to PS-PEG-OH micelles (Figures 5(a) and S23); the $R^{1/2}$ vs A profiles of PS-PEG and PtBMA-PEG micelles could also be reasonably modeled with eq 1 using a constant value of t over a wide range of A, again supporting the nondeformable and nondesorbing nature of these micelles.

Figures 5(b) and S25 display Π vs A and $R^{1/2}$ vs A plots for PiBMA-PEG micelles (having soft and strongly hydrophobic cores). The high-A portion of the $R^{1/2}$ vs A curve was fit to eq 1 by using M and t as adjustable parameters. A good fit was obtained at A > 420 cm² (i.e., before reaching the intermediate plateau at $\Pi \cong 27$ mN/m), with a thickness value of t = 5 nm. This t value is again significantly smaller than the core size ($D_c = 17.1$ nm). This thickness is also smaller than that determined

for PS-PEG-OH micelles (t = 8 nm), which supports the fact that, as discussed in Section 2.2, individual isolated PiBMA-PEG micelles had a flattened (oblate) core geometry (Figure 3(e)). Since PiBMA is more deformable ($T_g \cong 51$ °C in bulk), in the PiBMA-PEG case, it is reasonable to calculate t from measured R using eq 1 at a constant M. As shown in Figure 5(b), t was found to increase from 5 to 20 nm during compression across the intermediate plateau ($A \cong 260-420$ cm^2), which is in contrast to the constant t behavior seen in the cases of PS-PEG-OH and other rigid-core micelles in the same surface area range and suggests that the intermediate plateau occurred due to the deformation of the micelle core. As Π approached Π_{max} , t was seen to increase more rapidly with compression because of the collapse of the monolayer. We note that the constant *M* assumption used in the above analysis is reasonable because PiBMA-PEG micelles are not expected to easily desorb from the air-water interface. PnBMA-PEG and PB-PEG-OH micelles (having soft and strongly hydrophobic cores) also exhibited qualitatively similar reflectivity behaviors (Figures S26 and S28).

The $R^{1/2}$ vs A profiles of PMMA-PEG and PLA-PEG micelles having weakly hydrophobic cores could not be modeled using eq 1 under the assumption of constant Mbecause the high compression caused desorption of the micelles from the air-water interphase (Figures S27 and S29). Alternatively, for PLA-PEG micelles, for instance, M was calculated from measured R using eq 1 at constant t (Figure 6). As shown in the figure, M was found to decrease linearly with decreasing A, which indicates that the PLA-PEG micelles were indeed continuously lost to the subphase during compression. The polymer micelles in this subgroup (having nonstrongly hydrophobic cores) did not have sufficient affinity for the airwater interface to withstand the compressive stress beyond Π ≅ 10 mN/m. The core-cross-linked PB-PEG-OH micelles readily desorbed from the air-water interface even under moderate compression, as evidenced by nearly constant reflectivity (R) and also by the very low maximum surface pressure (Π) (Figure S30). This is understandable because

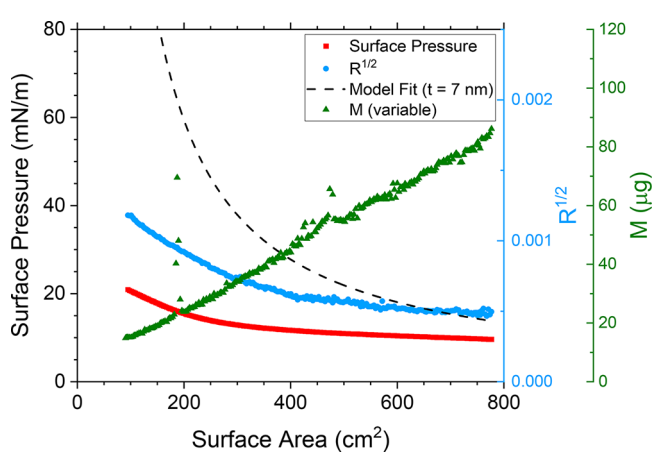


Figure 6. Surface pressure (Π, red squares) and square-root of reflectivity at the Brewster angle ($R^{1/2}$, blue circles) measured as functions of surface area (A) during compression at a barrier speed of 30 mm/min after 100 μ L of a 5 mg/mL PLA-PEG micelle solution in water was spread onto a clean water surface at an initial surface area of 777 cm². The dashed line represents values of $R^{1/2}$ computed using eq 1 at a constant optical thickness (t). The mass of PLA-PEG micelles adsorbed to the air—water interface (M, green triangles) was estimated from the $R^{1/2}$ data using eq 1. The linear decrease in M with decreasing A indicates a steady desorption of the micelles from the air—water interface during compression.

after the cross-linking treatment, anionic sulfonate $(-SO_4^-)$ moieties (from redox initiating agents) become incorporated into the surfaces of the PB core domains, and as a result, the micelles overall become more hydrophilic.

ADDITIONAL DISCUSSION

Figure 7 schematically summarizes our findings from this work. Figure 7(a) shows the responses of polymer micelles having rigid ($T_{\rm g} > 60~^{\circ}{\rm C}$) and strongly hydrophobic ($\theta > 80^{\circ}$) cores against lateral compression at the air—water interface; their behavior is similar to what has been reported for polymer brush-coated solid nanoparticles at the air—water interface. A7,48 During compression, the saturation of the air—water interface by adsorbed PEG chains produced a plateau in Π at $\Pi_{\rm e,PEG}$ ($\cong 10~{\rm mN/m}$) (at $a_{\rm m}/a_{\rm h} \approx 1$ –5). Further compression beyond $a_{\rm m}/a_{\rm h} \approx 1$ caused an overlap in the subphase PEG corona between adjacent micelles. The corresponding buildup of the osmotic pressure ($\Pi_{\rm osm} \sim c^y$) caused a rapid rise in Π (= $\Pi_{\rm e,PEG}$ + $\Pi_{\rm osm}$) and eventually the wrinkling and collapse of the monolayer at $a_{\rm m}/a_{\rm h} < 1$.

Figure 7(b) depicts the structural behavior of polymer micelles having soft (0 °C < $T_{\rm g}$ (in bulk) < 60 °C) and strongly hydrophobic ($\theta > 80^{\circ}$) cores at the air—water interface. There are two sets of data that suggest that these micelles assumed a flattened (oblate) shape after spreading on the water surface. The upturn in Π from the $\Pi_{\rm e,PEG}$ plateau in the Π vs $a_{\rm m}/a_{\rm h}$ plot occurred at a much higher surface area (i.e., at $a_{\rm m}/a_{\rm h} \approx 3$ for PiBMA-PEG and $a_{\rm m}/a_{\rm h} \approx 4$ for PnBMA-PEG) than that observed for spherical PS-PEG(-OH) and PtBMA-PEG micelles ($a_{\rm m}/a_{\rm h} \approx 1$). The thicknesses of these soft-core micelle monolayers ($t \cong 4-5$ nm) estimated by QBAM measurements were much smaller than those obtained for rigid-core PS-PEG(-OH)/PtBMA-PEG micelles with comparable core diameters ($t \cong 8-11$ nm). Also, in these soft-core cases, an additional intermediate-Π plateau was observed (at $\Pi \cong 27$ mN/m for PiBMA-PEG and $\Pi \cong 23$

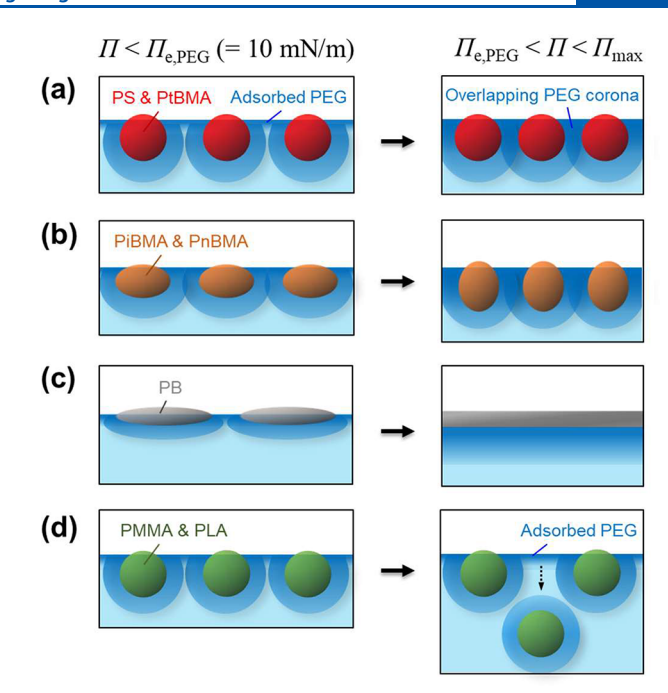


Figure 7. Schematic illustration of what happens to water-spread PEG-based block copolymer (BCP) micelles at the air—water interface under high compression. (a) BCP micelles with very hydrophobic, rigid nondeformable cores. (b) BCP micelles with very hydrophobic, soft deformable cores. (c) BCP micelles with very hydrophobic, liquid-like cores. (d) BCP micelles with less hydrophobic cores.

mN/m for PnBMA-PEG) likely because of the transformation of the shape of the micelle cores from oblates to spheres (even to prolates) during compression. However, PiBMA-PEG and PnBMA-PEG micelles did not seem to coalesce even at very high Π (>60 mN/m). Instead, the PiBMA-PEG and PnBMA-PEG micelle monolayers became collapsed under high compression. In contrast, PB-PEG-OH micelles having liquid-like cores ($T_{\rm g}\cong -3$ °C in bulk, $\theta\cong 96$ °) turned into a continuous film at $a_m/a_h < 2$ because of the strong tendency of PB to wet the water surface (Figure 7(c)). PMMA-PEG and PLA-PEG micelles having weakly hydrophobic (θ < 80°) cores were found to desorb from the air-water interface at $\Pi \ge$ $\Pi_{e,PEG}$ (Figure 7(d)), which prevented them from producing high Π . We wish to highlight, as evident in Figure 6, that the desorption of micelles with less hydrophobic cores is initiated at relatively lower surface micelle concentrations, notably within the 2D PEG "mushroom-to-pancake" transition region (at $\Pi \cong \Pi_{e,PEG} \cong 10 \text{ mN/m}$). This observation has been incorporated into the visualization presented in the right-hand cartoon of Figure 7(d), where adjacent micelles are depicted as somewhat spaced apart and the 2D "pancake" layer of PEG consistently blankets the water surface, irrespective of the desorption of micelles.

Finally, let us discuss which of the tested block copolymers are in fact suitable for use as a surfactant replacement therapy for treating respiratory distress syndrome (such as ARDS). A successful polymer lung surfactant (PLS) candidate should be able to produce high surface pressure (>60 mN/m) at high compression in order to help reduce respiratory work (especially at end-expiration). As summarized in Table 2, PS-PEG(-OH), PtBMA-PEG, PiBMA-PEG, and PnBMA-PEG micelles (i.e., polymer micelles having rigid, or at least only

slightly soft, and strongly hydrophobic cores) were found to satisfy this high surface pressure requirement. Additionally, a PLS candidate should be able to stabilize alveoli against collapse/overdistention (that occurs due to an imbalance in Laplace pressure (ΔP) among differently sized alveoli) by appropriately varying the alveolar air-water interfacial tension (γ) (Figure 1(a)). Recently, it has been proposed that the mechanical stability of alveolar tissue is ensured when ΔP is regulated such that $d(\Delta P)/dr < 0$ (where r is the radius of the alveolus) at all times during the breathing cycle; it can be shown that, in the small and slow deformation limit with negligible bending stress, substitution of the Young-Laplace equation $(\Delta P = 2\gamma/r)$ into the above stability criterion yields an alternative expression, $2E > \gamma$ (where $E = A(\partial \gamma / \partial A)$). Assuming that our measured surface tension values (obtained using a Wilhelmy plate in a Langmuir trough) represent equilibrium surface tension values, our surface pressure-area isotherm data can be further analyzed against this alveolar stability criterion. In the E vs Π plots shown in Figures 2(d) and 3(d), the limits of alveolar stability ($2E = \gamma$, that is, $2E = \gamma_0$ $-\Pi$) are shown using red dotted lines; in the region above this line, the polymer micelles satisfy the Laplace stability requirement. As shown in Figure 2(d), in the cases for micelles having rigid and strongly hydrophobic cores (PS-PEG(-OH) and PtBMA-PEG micelles), the $2E - \gamma$ values were positive over most of the range of Π because of the continuous increase of E with Π ; these micelles would be able to mechanically stabilize the alveoli. On the other hand, in the cases of micelles having soft and strongly hydrophobic cores (PiBMA-PEG and PnBMA-PEG micelles), the region of positive $2E - \gamma$ became significantly reduced because of the existence of the intermediate-Π plateau (Figure 3(d)). PLA-PEG micelles having weakly hydrophobic cores and also PB-PEG-OH micelles having liquid-like cores were unable to produce positive $2E - \gamma$ values under all conditions because their E_{max} values were too low. Taken together, PS-PEG(-OH) and PtBMA-PEG micelles (having rigid and strongly hydrophobic cores) appear to be the most appropriate for use as a lung surfactant.

CONCLUSIONS

Micelles derived from amphiphilic block copolymers are promising materials for surfactant replacement therapy applications. In surfactant replacement therapy, the surfacetension-regulating ability of a surfactant is key to producing therapeutic effects. In order to better understand factors controlling the surface tension behavior of water-spread block copolymer micelles at the air-water interface, we prepared eight different PEG-based block copolymers having a comparable overall molecular weight and hydrophilic/hydrophobic block composition but having different hydrophobic block chemistries (PS-PEG, PS-PEG-OH, PtBMA-PEG, PiBMA-PEG, PnBMA-PEG, PMMA-PEG, PLA-PEG, and PB-PEG-OH) and investigated their micellar surface mechanical and monolayer morphological properties by surface tension-area isotherm and quantitative Brewster angle microscopy measurements. We found that the rigidity (glasstransition temperature (Tg)) and degree of hydrophobicity (water contact angle (θ)) of the micelle core domain are two key factors that predominantly determine the surface mechanical behavior of the micelle monolayer through their influence on the interfacial affinity and deformability of the micelle structure under lateral compression. PS-PEG(-OH)

and PtBMA-PEG micelles having rigid (high T_g) and strongly hydrophobic (high θ) cores produced high surface pressure (Π) and a high compressibility modulus (E) under high compression because these micelles have a strong affinity for the air-water interface while at the same time their core domains are mechanically rigid, and as a result, these micelles are able to sustain a buildup of PEG osmotic pressure during compression. Also, for the same reason, PS-PEG(-OH)/ PtBMA-PEG micelle monolayers became wrinkled or collapsed when further compressed beyond a certain limit. PiBMA-PEG and PnBMA-PEG micelles having soft (lower T_g) and strongly hydrophobic (high θ) cores were also able to produce reasonably high surface pressure, but, on the other hand, these micelles were found to undergo deformation (vertical elongation) under compression, which was manifested as an intermediate plateau in Π. PB-PEG-OH micelles having liquidlike (very low $T_{\rm g}$) and strongly hydrophobic (high $\tilde{\theta}$) cores became merged into a continuous film under compression because PB has a strong tendency to wet the air-water interface. For this reason, high surface pressure was not achievable with this material. PMMA-PEG and PLA-PEG micelles having weakly hydrophobic (lower θ) cores did not have enough affinity for the air-water interface and were prone to desorption under compression and thus unable to produce high surface pressure. Taken together, block copolymer micelles with rigid and strongly hydrophobic cores appear to be good candidates for use as lung surfactants.

EXPERIMENTAL SECTION

Synthesis and Characterization of Polymers Tested. PS-PEG-OH and PB-PEG-OH were purchased from PolymerSource; according to the vendor, these polymers were synthesized by living anionic polymerization, and the PEG blocks of these block copolymers have hydroxyl end groups. All other block copolymers used in this study were synthesized in our laboratory using a commercial monomethoxy/monohydroxy-terminated PEG (5.0 kDa, Sigma-Aldrich) as a precursor. PS-PEG and poly(alkyl methacrylate)-PEG block copolymers were synthesized by reversible additionfragmentation (chain) transfer polymerization (RAFT) using procedures described in ref 50. PLA-PEG was synthesized by 1,8diazabicyclo[5.4.0]undec-7-ene (DBU)-catalyzed ring-opening polymerization.⁵¹ PS and poly(alkyl methacrylate) homopolymers were also synthesized similarly by RAFT using 4-cyano-4-[(dodecylsulfanylthiocarbonyl)sulfanyl]pentanoic acid (CDSP) as the RAFT agent.

The molecular weights (Mn values) of the polymers were determined by ¹H NMR (Figures S1-S6 in the Supporting Information (SI) for block copolymers and Figures S9-S13 for homopolymers). The polydispersity indices of the polymers (D = 0 $M_{\rm w}/M_{\rm p}$) were determined by gel permeation chromatography (GPC) (Figure S14 for diblock copolymers and Figure S15 for homopolymers). The glass-transition temperatures (T_g values) of the homopolymers were determined by differential scanning calorimetry (DSC) (Figure S16). The advancing water contact angles (θ) were measured on spin-coated homopolymer films by the sessile drop technique (Figure S17). The molecular characteristics of all block copolymers and homopolymers used are summarized in Table S1 of the SI. The exact chemical structures of the polymers used are also shown in Figures S1-S6 (block copolymers) and Figures S9-S13 (homopolymers). Detailed procedures for polymer synthesis and characterization are described in Section S1 of the SI. We note that in the GPC measurements for some of the block copolymers (i.e., PiBMA-PEG, and PMMA-PEG) the presence of lower-molecularweight shoulders was observed (Figure S14(B)). As shown in Figure S7, the CDSP end functionality of the PEG-CDSP macro-RAFT agent was close to 100%. Therefore, the lower-molecular-weight

shoulders are thought to be the result of dead polymer chains formed during the RAFT polymerization process (rather than unreacted PEG chains). Regardless of the nature of these lower-molecular-weight fractions, they should not have influenced the surface mechanical behavior of the block copolymer micelles. Any hydrophobic homopolymers would have been incorporated into the core domains of the micelles. As demonstrated in Figure S8, the coexistence of PEG homopolymer chains was also confirmed not to affect the structural or surface mechanical properties of copolymer micelles.

Formulation of Block Copolymer Micelles. Block copolymer micelles were prepared using the equilibrium nanoprecipitation (ENP) procedure.¹¹ Briefly, micellization was initially induced by adding water to a block copolymer solution in acetone. This micelle solution was equilibrated at room temperature for 24 h. The solvent composition was adjusted to minimize the size polydispersity of the micelles; as shown in Table 2, the optimal solvent composition $(\phi_{\mathrm{w.ENP}})$ varied from block copolymer to block copolymer. After the equilibration step, acetone was removed from the micelle solution via dialysis against pure water. The block copolymer micelles thus prepared were confirmed to be stable in water for at least 3 weeks when stored at 4 $^{\circ}$ C. The core diameters of polymer micelles (D_c) were measured by transmission electron microscopy (TEM) (Figure \$18). TEM measurements were made using dried micelle specimens collected on carbon-coated TEM grids. In the case of PB-PEG-OH micelles, TEM was performed after the PB core was chemically crosslinked using the literature procedure. 52 The hydrodynamic diameters (D_h) and polydispersity indices (PDI = 2 μ/Γ^2 , where Γ and μ are the first and second cumulants of the DLS autocorrelation function) of the polymer micelles were measured by dynamic light scattering (DLS). Detailed procedures for micelle formulation and characterization are described in Section S2 of the SI.

Surface Pressure-Area Isotherm and Brewster Angle **Microscopy Measurements.** Surface pressure—area $(\Pi - A)$ isotherms for block copolymer micelles were obtained using a KSV 5000 Langmuir trough with two symmetric Delrin barriers (Biolin Scientific). The trough temperature was controlled by using a circulating water bath. All measurements were performed at 25 °C. The trough and barriers were initially cleaned with ethanol and Milli-Q water. Then, the trough was filled with 1.4 L of water and the barriers were mounted. The surface tension was measured by using a filter paper Wilhelmy plate facing the direction of the compression. The water surface was aspirated to remove contaminants until the surface pressure increase during a blank compression ($A = 782 \rightarrow 71$ cm²) did not exceed 0.2 mN/m. Afterward, 10 or 100 μ L of a polymer micelle solution was spread to a surface area of water of $A = 782 \text{ cm}^2$ using a 50 μ L Hamilton syringe. An ~2 μ L drop of a micelle solution (5.0 mg/mL) that formed at the tip of the syringe needle was carefully contacted with water to spread polymer micelles on the water surface. After 10 min of equilibration, the Π -A isotherm measurement was conducted during compression at a barrier speed of 3 mm/min. The Π readings were recalibrated to account for the swelling of the filter paper in water (i.e., to correct for the true perimeter of the waterswollen filter paper, as described in our previous publication¹¹). The original $\Pi - A$ isotherms were converted to $\Pi - a_{\rm m}$ isotherms; note that $a_{\rm m}$ (surface area per micelle) = A/N, where N (number of micelles spread) = cVN_A/pM_n . For each block copolymer, the two $\Pi-a_m$ isotherm curves (obtained using the two different amounts of spreading solution, i.e., 10 vs 100 μ L) were superposed by shifting the isotherm obtained with 100 μ L of spreading along the $a_{\rm m}$ axis to make it overlap with the isotherm obtained with 10 μ L spreading.

Brewster angle microscopy (BAM) measurements were performed by using an UltraBAM instrument (Accurion) hosted on a KSV NIMA two-barrier Langmuir trough platform (Biolin Scientific). The general trough operating procedures were similar to the above. The spreading volume was 100 μ L. After equilibration for 10 min, the micelle monolayer was compressed from A = 777 cm² to A = 90 cm² at a barrier speed of 30 mm/min, and during the compression, the surface pressure values and BAM images were simultaneously recorded every 1 s. BAM images were collected at a lateral resolution of 2 μ m in a field of view (FOV) of $800 \times 430 \ \mu$ m², and a region of

interest (ROI) of 100 \times 100 μm^2 located at the center of the FOV was analyzed for the determination of the reflectivity of the micelle-laden air—water interface. The intensity of the reflected p-polarized light ($\lambda=658$ nm) from the micelle-laden water surface at the Brewster angle of water (= 53.1°) was measured and converted to an absolute reflectivity scale using a calibration procedure that utilizes the null-surface (pure water) reflectivity data obtained at a series of angles in the range of $53.1\pm0.5^\circ$.

ASSOCIATED CONTENT

Supporting Information

The Supporting Information is available free of charge at https://pubs.acs.org/doi/10.1021/acs.langmuir.3c01574.

Molecular characteristics of the homopolymers (Table S1, Figures S9–S13, and Figures S15–S16) and block copolymers (Figures S1–S7 and Figure S14); supplementary surface pressure—area isotherms (Figures S8, S19–S21); water contact angle measurements (Figure S17); TEM characterization of the micelles (Figure S18); and quantitative BAM analysis (Figures S22–S30) (PDF)

AUTHOR INFORMATION

Corresponding Author

You-Yeon Won — Davidson School of Chemical Engineering, Purdue University, West Lafayette, Indiana 47907, United States; Purdue University Institute for Cancer Research, Purdue University, West Lafayette, Indiana 47907, United States; orcid.org/0000-0002-8347-6375; Phone: +1-765-494-4077; Email: yywon@purdue.edu; Fax: +1-765-494-0805

Authors

Seyoung Kim — Davidson School of Chemical Engineering, Purdue University, West Lafayette, Indiana 47907, United States; Department of Polymer Science and Engineering, Dankook University, Yongin, Gyeonggi 16890, Republic of Korea

Sungwan Park – Davidson School of Chemical Engineering, Purdue University, West Lafayette, Indiana 47907, United States

Daniel J. Fesenmeier — Davidson School of Chemical Engineering, Purdue University, West Lafayette, Indiana 47907, United States

Taesuk Jun – Davidson School of Chemical Engineering, Purdue University, West Lafayette, Indiana 47907, United States

Kaustabh Sarkar — Davidson School of Chemical Engineering, Purdue University, West Lafayette, Indiana 47907, United States

Complete contact information is available at: https://pubs.acs.org/10.1021/acs.langmuir.3c01574

Notes

The authors declare no competing financial interest.

ACKNOWLEDGMENTS

The authors are grateful for funding from ACS PRF (60233-ND7), NSF (IIP-2036125, CBET-2211843), and Spirrow Therapeutics. The authors also acknowledge support from the Purdue University Institute for Cancer Research (PU-ICR) via an NIH NCI grant (P30 CA023168), which supports the

campus-wide NMR shared resources that were utilized in this work.

REFERENCES

- (1) Harayama, T.; Riezman, H. Understanding the Diversity of Membrane Lipid Composition. *Nat. Rev. Mol. Cell Biol.* **2018**, *19*, 281–296.
- (2) Zuo, Y. Y.; Veldhuizen, R. A. W.; Neumann, A. W.; Petersen, N. O.; Possmayer, F. Current Perspectives in Pulmonary Surfactant Inhibition, Enhancement and Evaluation. *Biochim. Biophys. Acta Biomembr.* **2008**, *1778*, 1947–1977.
- (3) Zhang, H.; Wang, Y. E.; Fan, Q.; Zuo, Y. Y. On the Low Surface Tension of Lung Surfactant. *Langmuir* 2011, 27, 8351–8358.
- (4) Witte, K. N.; Kewalramani, S.; Kuzmenko, I.; Sun, W.; Fukuto, M.; Won, Y.-Y. Formation and Collapse of Single-Monomer-Thick Monolayers of Poly(n-Butyl Acrylate) at the Air-Water Interface. *Macromolecules* **2010**, *43*, 2990–3003.
- (5) Park, H. W.; Choi, J.; Ohn, K.; Lee, H.; Kim, J. W.; Won, Y.-Y. Study of the Air-Water Interfacial Properties of Biodegradable Polyesters and Their Block Copolymers with Poly(Ethylene Glycol). *Langmuir* **2012**, 28, 11555–11566.
- (6) Kim, H. C.; Lee, H.; Jung, H.; Choi, Y. H.; Meron, M.; Lin, B.; Bang, J.; Won, Y.-Y. Humidity-Dependent Compression-Induced Glass Transition of the Air-Water Interfacial Langmuir Films of Poly(D,L-lactic acid-ran-glycolic acid) (PLGA). Soft Matter 2015, 11, 5666–5677.
- (7) Kim, H. C.; Lee, H.; Khetan, J.; Won, Y. Y. Surface Mechanical and Rheological Behaviors of Biocompatible Poly((D,L-lactic acid-ran-glycolic acid)-block-ethylene glycol) (PLGA-PEG) and Poly-((D,L-lactic acid-ran-glycolic acid-ran-ε-caprolactone)-block-ethylene glycol) (PLGACL-PEG) Block Copolymers at the Air-Water Interface. Langmuir 2015, 31, 13821–13833.
- (8) Kim, H. C.; Arick, D. Q.; Won, Y.-Y. Air-Water Interfacial Properties of Chloroform-Spread versus Water-Spread Poly((D,L-lactic acid-*ran*-glycolic acid)-*block*-ethylene glycol) (PLGA-PEG) Polymers. *Langmuir* **2018**, *34*, 4874–4887.
- (9) Kim, H. C.; Suresh, M. V.; Singh, V. V.; Arick, D. Q.; Machado-Aranda, D. A.; Raghavendran, K.; Won, Y.-Y. Polymer Lung Surfactants. ACS Appl. Bio Mater. 2018, 1, 581–592.
- (10) Fesenmeier, D. J.; Suresh, M. V.; Kim, S.; Park, S.; Raghavendran, K.; Won, Y.-Y. Polymer Lung Surfactants Attenuate Direct Lung Injury in Mice. ACS Biomater. Sci. Eng. 2023, 9, 2716–2730.
- (11) Fesenmeier, D. J.; Park, S.; Kim, S.; Won, Y.-Y. Surface Mechanical Behavior of Water-Spread Poly(styrene)-Poly(ethylene glycol) (PS-PEG) Micelles at the Air-Water Interface: Effect of Micelle Size and Polymer End/Linking Group Chemistry. J. Colloid Interface Sci. 2022, 617, 764–777.
- (12) Dushianthan, A.; Cusack, R.; Goss, V.; Postle, A. D.; Grocott, M. P. W. Clinical Review: Exogenous Surfactant Therapy for Acute Lung Injury/Acute Respiratory Distress Syndrome Where Do We Go from Here? *Crit. Care* **2012**, *16*, 238.
- (13) Willson, D. F.; Notter, R. H. The Future of Exogenous Surfactant Therapy. *Respir. Care* **2011**, *56*, 1369–1388.
- (14) Kim, H. C.; Won, Y.-Y. Clinical, Technological, and Economic Issues Associated with Developing New Lung Surfactant Therapeutics. *Biotechnol. Adv.* **2018**, *36*, 1185–1193.
- (15) Barman, S.; Davidson, M. L.; Walker, L. M.; Anna, S. L.; Zasadzinski, J. A. Inflammation Product Effects on Dilatational Mechanics Can Trigger the Laplace Instability and Acute Respiratory Distress Syndrome. *Soft Matter* **2020**, *16*, 6890–6901.
- (16) Israelachvili, J. Intermolecular and Surface Forces; Academic Press: Waltham, MA, 2011; pp 535–576.
- (17) Hórvölgyi, Z.; Máté, M.; Dániel, A.; Szalma, J. Wetting Behaviour of Silanized Glass Microspheres at Water-Air Interfaces: A Wilhelmy Film Balance Study. *Colloids Surfaces A Physicochem. Eng. Asp.* 1999, 156, 501–507.
- (18) Geisel, K.; Rudov, A. A.; Potemkin, I. I.; Richtering, W. Hollow and Core-Shell Microgels at Oil-Water Interfaces: Spreading of Soft

- Particles Reduces the Compressibility of the Monolayer. *Langmuir* **2015**, *31*, 13145–13154.
- (19) Matthay, M. A.; Zemans, R. L. The Acute Respiratory Distress Syndrome: Pathogenesis and Treatment. *Annu. Rev. Pathol. Mech. Dis.* **2011**, *6*, 147–163.
- (20) Sasannejad, C.; Ely, E. W.; Lahiri, S. Long-Term Cognitive Impairment after Acute Respiratory Distress Syndrome: A Review of Clinical Impact and Pathophysiological Mechanisms. *Crit. Care* **2019**, 23, 352.
- (21) Wu, S. Polymer Interface and Adhesion; Marcel Dekker: New York, 1982; pp 133-168.
- (22) Vargha-Butler, E. I.; Kiss, E.; Lam, C. N. C.; Keresztes, Z.; Kálmán, E.; Zhang, L.; Neumann, A. W. Wettability of Biodegradable Surfaces. *Colloid Polym. Sci.* **2001**, *279*, 1160–1168.
- (23) Vargaftik, N. B.; Volkov, B. N.; Voljak, L. D. International Tables of the Surface Tension of Water. *J. Phys. Chem. Ref. Data* **1983**, 12, 817–820.
- (24) Kim, S.; Lee, M.; Kim, H. C.; Kim, Y. J.; Lee, W. B.; Won, Y.-Y. Determination of Glass Transition Temperatures in Bulk and Micellar Nanoconfined Polymers by Using Fluorescent Molecular Rotors as Probes for Changes in Free Volume. *Macromolecules* **2023**, *56* (16), 6290–6304.
- (25) Blasi, P.; D'Souza, S. S.; Selmin, F.; DeLuca, P. P. Plasticizing Effect of Water on Poly(lactide-co-glycolide). *J. Controlled Release* **2005**, *108*, 1–9.
- (26) Yamamoto, S.; Tsujii, Y.; Fukuda, T. Glass Transition Temperatures of High-Density Poly(methyl methacrylate) Brushes. *Macromolecules* **2002**, *35*, 6077–6079.
- (27) Dormidontova, E. E. Micellization Kinetics in Block Copolymer Solutions: Scaling Model. *Macromolecules* **1999**, 32, 7630–7644.
- (28) Cao, B. H.; Kim, M. W. Molecular Weight Dependence of the Surface Tension of Aqueous Poly(ethylene oxide) Solutions. *Faraday Discuss.* **1994**, *98*, 245.
- (29) Zell, Z. A.; Isa, L.; Ilg, P.; Leal, L. G.; Squires, T. M. Adsorption Energies of Poly(ethylene oxide)-Based Surfactants and Nanoparticles on an Air-Water Surface. *Langmuir* **2014**, *30*, 110–119.
- (30) Rubinstein, M.; Colby, R. H. *Polymer Physics*; Oxford University Press: Oxford, U.K., 2003; pp 181–182.
- (31) Vilanove, R.; Rondelez, F. Scaling Description of Two-Dimensional Chain Conformations in Polymer Monolayers. *Phys. Rev. Lett.* **1980**, *45*, 1502–1505.
- (32) Kawaguchi, M.; Komatsu, S.; Matsuzumi, M.; Takahashi, A. Concentration Dependence of Surface Pressure of Polyether Monolayers at the Air-Water Interface. *J. Colloid Interface Sci.* **1984**, 102, 356–360.
- (33) Menath, J.; Eatson, J.; Brilmayer, R.; Andrieu-Brunsen, A.; Buzza, D. M. A.; Vogel, N. Defined Core-Shell Particles as the Key to Complex Interfacial Self-Assembly. *Proc. Natl. Acad. Sci. U.S.A.* **2021**, *118*, No. e2113394118.
- (34) Kuzmenka, D. J.; Granick, S. Collapse of Poly(ethylene oxide) Monolayers. *Macromolecules* **1988**, 21, 779–782.
- (35) Kawaguchi, S.; Imai, G.; Suzuki, J.; Miyahara, A.; Kitano, T.; Ito, K. Aqueous Solution Properties of Oligo- and Poly(ethylene oxide) by Static Light Scattering and Intrinsic Viscosity. *Polymer* 1997, 38, 2885–2891.
- (36) Lee, H.; Kim, D. H.; Park, H. W.; Mahynski, N. A.; Kim, K.; Meron, M.; Lin, B.; Won, Y.-Y. Reduced Water Density in a Poly(ethylene oxide) Brush. *J. Phys. Chem. Lett.* **2012**, *3*, 1589–1595.
- (37) Lee, H.; Kim, D. H.; Witte, K. N.; Ohn, K.; Choi, J.; Akgun, B.; Satija, S.; Won, Y.-Y. Water Is a Poor Solvent for Densely Grafted Poly(ethylene oxide) Chains: A Conclusion Drawn from a Self-Consistent Field Theory-Based Analysis of Neutron Reflectivity and Surface Pressure-Area Isotherm Data. J. Phys. Chem. B 2012, 116, 7367–7378.
- (38) Deshmukh, O. S.; Maestro, A.; Duits, M. H. G.; Van Den Ende, D.; Stuart, M. C.; Mugele, F. Equation of State and Adsorption Dynamics of Soft Microgel Particles at an Air-Water Interface. *Soft Matter* **2014**, *10*, 7045–7050.

- (39) Rey, M.; Fernandez-Rodriguez, M. A.; Karg, M.; Isa, L.; Vogel, N. Poly-*N*-isopropylacrylamide Nanogels and Microgels at Fluid Interfaces. *Acc. Chem. Res.* **2020**, *53*, 414.
- (40) Burroughs, M. J.; Christie, D.; Gray, L. A. G.; Chowdhury, M.; Priestley, R. D. 21st Century Advances in Fluorescence Techniques to Characterize Glass-Forming Polymers at the Nanoscale. *Macromol. Chem. Phys.* **2018**, 219, 1700368.
- (41) Roth, C. B. Polymers under Nanoconfinement: Where Are We Now in Understanding Local Property Changes? *Chem. Soc. Rev.* **2021**, *50*, 8050–8066.
- (42) Matmour, R.; Joncheray, T. J.; Gnanou, Y.; Duran, R. S. Two-Dimensional Polymeric Nanomaterials through Cross-Linking of Polybutadiene-b-Poly(ethylene oxide) Monolayers at the Air/Water Interface. *Langmuir* **2007**, 23, 649–658.
- (43) Murphy, R. P.; Kelley, E. G.; Rogers, S. A.; Sullivan, M. O.; Epps, T. H. Unlocking Chain Exchange in Highly Amphiphilic Block Polymer Micellar Systems: Influence of Agitation. *ACS Macro Lett.* **2014**, *3*, 1106–1111.
- (44) Lee, L.-H. Adhesion of High Polymers. II. Wettability of Elastomers. J. Polym. Sci. Part A-2 Polym. Phys. 1967, 5, 1103–1118.
- (45) Carey, D. H.; Ferguson, G. S. Synthesis and Characterization of Surface-Functionalized 1,2-Polybutadiene Bearing Hydroxyl or Carboxylic Acid Groups. *Macromolecules* 1994, 27, 7254–7266.
- (46) Fernsler, J. G.; Zasadzinski, J. A. Competitive Adsorption: A Physical Model for Lung Surfactant Inactivation. *Langmuir* **2009**, 25, 8131–8143
- (47) Schwenke, K.; Isa, L.; Cheung, D. L.; Del Gado, E. Conformations and Effective Interactions of Polymer-Coated Nanoparticles at Liquid Interfaces. *Langmuir* **2014**, *30*, 12578–12586.
- (48) Rauh, A.; Rey, M.; Barbera, L.; Zanini, M.; Karg, M.; Isa, L. Compression of Hard Core-Soft Shell Nanoparticles at Liquid-Liquid Interfaces: Influence of the Shell Thickness. *Soft Matter* **2017**, *13*, 158–169.
- (49) Notter, R. H. Lung Surfactants: Basic Science and Clinical Applications; Marcel Dekker: New York, 2000; pp 121–127.
- (50) Kim, S.; Fesenmeier, D. J.; Park, S.; Torregrosa-Allen, S. E.; Elzey, B. D.; Won, Y.-Y. Pulmonary Pharmacokinetics of Polymer Lung Surfactants Following Pharyngeal Administration in Mice. *Biomacromolecules* **2022**, 23, 2471–2484.
- (51) Sarkar, K.; Torregrossa-Allen, S. E.; Elzey, B. D.; Narayanan, S.; Langer, M. P.; Durm, G. A.; Won, Y.-Y. Effect of Paclitaxel Stereochemistry on X-Ray-Triggered Release of Paclitaxel from CaWO4/Paclitaxel-Coloaded PEG-PLA Nanoparticles. *Mol. Pharmaceutics* **2022**, *19*, 2776–2794.
- (52) Won, Y.-Y.; Paso, K.; Ted Davis, H.; Bates, F. S. Comparison of Original and Cross-Linked Wormlike Micelles of Poly(ethylene oxide-b-butadiene) in Water: Rheological Properties and Effects of Poly(ethylene oxide) Addition. *J. Phys. Chem. B* **2001**, *105*, 8302–8311.